

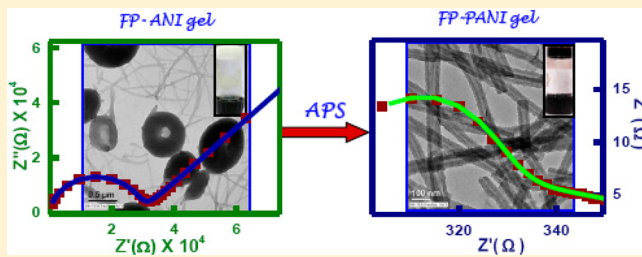
# Co-Assembled Conductive Hydrogel of *N*-Fluorenylmethoxycarbonyl Phenylalanine with Polyaniline

Priyadarshi Chakraborty, Partha Bairi, Sanjoy Mondal, and Arun K. Nandi\*

Polymer Science Unit, Indian Association for the Cultivation of Science, Jadavpur, Kolkata 700 032, India

## S Supporting Information

**ABSTRACT:** A metastable coassembled hydrogel of *N*-Fluorenylmethoxycarbonyl (Fmoc) phenylalanine (FP) with aniline (FP-ANI), upon polymerization, produces a stable green-colored coassembled FP-polyaniline (FP-PANI) hydrogel. The coassembly is produced by supramolecular interactions between FP and ANI/PANI. WAXS spectra suggest that structures of FP powder, FP-ANI, and FP-PANI xerogels are different from each other. The FP-ANI gel exhibits a mixture of doughnut and fiber morphology, but the FP-PANI gel exhibits a nanotubular morphology. UV-vis spectroscopy suggests that the doped state of PANI and the fluorescence property of FP completely vanish in the FP-PANI gel. The storage and loss modulii ( $G'$  and  $G''$ ) of the FP-PANI gel are higher than those of the FP-ANI gel. The FP-ANI gel breaks at a lower oscillator stress (57 Pa) than the FP-PANI gel (93 Pa), which exhibits a good strain recovery demonstrating excellent viscoelastic properties. The FP-PANI gel also exhibits a dc conductivity ( $1.2 \times 10^{-2} \text{ S}\cdot\text{cm}^{-1}$ ) that is seven orders higher than that of the FP-ANI gel because of the doped nature of PANI. The current-voltage ( $I-V$ ) characteristic curve of FP-PANI xerogel resembles the behavior of a semiconductor-metal junction, and upon white light irradiation, it exhibits a reversible on-off cycle with a constant photocurrent value of 0.1 mA. The Nyquist plot obtained from impedance measurements of the FP-PANI xerogel is different from that obtained for the FP-ANI xerogel, and it exhibits almost a semicircle, indicating the existence of both resistive and capacitive features connected in parallel mode.



## INTRODUCTION

Hydrogels are a class of cross-linked supramolecular networks that can gelatinize water, forming an entangled three-dimensional network with a high surface area. Currently, supramolecular hydrogels are gaining substantial research interest because they can be used for a plethora of technological appliances in drug delivery,<sup>1,2</sup> tissue engineering,<sup>3–5</sup> pollutant capture and release,<sup>6–8</sup> templated nanomaterial syntheses,<sup>9</sup> microarray kit design,<sup>10</sup> and sensing and soft lithography.<sup>11</sup> They are advantageous in many ways because they are thermoreversible, highly tunable, and stimuli-responsive.<sup>12,13</sup> However, their mechanical stability is limited because of the weak intermolecular physical forces holding the components together. Therefore, it is a profound challenge to combine the mechanical stability and robustness of covalent structures with the reversibility and external switchability of supramolecular gels.

Recently, electroresponsive hydrogels have emerged as a new area of intense research because of their potential use in drug release, bioactive electrodes, coatings, and actuators.<sup>14–16</sup> They can be engineered by myriad processes such as adding conductive particles to the gel matrix,<sup>17</sup> producing gels directly from conducting polymers,<sup>18–24</sup> or incorporating conducting polymers into the network structure of gels.<sup>25,26</sup> Some groups have reported fabrication of conductive hydrogels by in situ polymerization of the monomers inside the gel matrix.<sup>27–30</sup>

Recently, Xia and Zhu reported a novel composite hydrogel embedded with polyaniline (PANI) nanofibers, fabricated by means of rapid polymerization of aniline in a poly(acrylic acid) (PAA) hydrogel.<sup>31</sup> The composite hydrogel displayed good conductive properties, enhanced mechanical strength, and unique pH sensitivity. However, in all of the above reports of in situ polymerization, the gel matrixes are polymer gels and not supramolecular gels. In situ polymerization of aniline in a supramolecular gel matrix has rarely been reported in literature.<sup>32–34</sup> In all of these reports, the supramolecular gels have been used as templates, and the mechanical properties of the gels after polymerization have scarcely been investigated. Recently, in an elegant work, we reported a coassembled gel of folic acid and polyaniline in a water/dimethyl sulfoxide (1:1, v/v) mixture by in situ polymerization of aniline.<sup>35</sup> The folic acid–polyaniline coassembled gel exhibited much improved mechanical and electronic properties compared to the parent gel.

*N*-Fluorenylmethoxycarbonyl (Fmoc) phenylalanine (FP) is a well-known Fmoc-protected essential amino acid that forms a hydrogel with the help of H-bonding as well as  $\pi$ -stacking interactions.<sup>36–38</sup> We reported a coassembled organogel of FP

Received: August 26, 2014

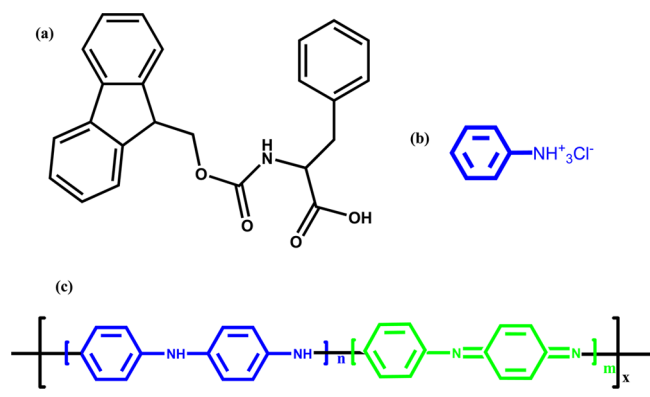
Revised: November 7, 2014

Published: November 10, 2014

with 2-aminoanthracene (AA) and 2-aminonaphthalene (NA) at a 1:1 molar ratio of the components. The FP–AA organogel showed improved mechanical properties compared to the FP gel and a signature of negative differential resistance in the *I*–*V* characteristic curves.<sup>39</sup> In the present study, we were interested in coassembling this important amino acid with a conducting polymer to import new electronic properties along with improved mechanical properties. Polyaniline is the most common member among the conducting polymer family, but it faces some disadvantages such as solubility in common organic solvents and poor mechanical properties for its application. Therefore, the objective of this work was to solve the processability problem of PANI and also to impart good mechanical properties by making a coassembled hydrogel with FP. These conducting soft materials are expected to be very useful for the fabrication of optoelectronic, soft electronic, and biosensing devices.<sup>40–42</sup> Therefore, it would be very interesting to produce a coassembled hydrogel that is electrically conducting and simultaneously mechanically strong.

In this work, we have prepared a metastable coassembled hydrogel of FP with aniline (FP–ANI) (Scheme 1) by

**Scheme 1. Chemical Structures of (a) Fmoc-Phenylalanine, (b) Anilinium Chloride, and (c) Polyaniline (Emeraldine Base Form)**



dissolving FP in the required quantity of NaHCO<sub>3</sub> solution and then added a solution of anilinium chloride to this basic solution of FP, after which instant gel formation was observed. The FP–ANI gel, when polymerized with an aqueous solution of ammonium persulfate (APS), gives rise to a green-colored FP–PANI gel with an interesting nanotubular morphology. This FP–PANI hydrogel is stable for months and shows improved mechanical properties compared to those of the FP–ANI gel. The xerogel exhibits a dc conductivity of  $1.15 \times 10^{-2}$  S/cm, and its *I*–*V* characteristic curve resembles that of a semimetal. We also used impedance spectroscopy for the nondestructive characterization of the xerogel from the electrochemical viewpoint and found that the Nyquist plot reflects the existence of a circuit having a parallel combination of capacitance and resistance in both systems.

## ■ EXPERIMENTAL METHODS

**Materials.** N-Fluorenylmethoxycarbonyl phenylalanine (FP) was purchased from Aldrich Chemical Co. (Milwaukee, WI) and used without further purification. Ammonium persulfate (APS) was purchased from Merck Chemicals (Mumbai, India) and used as received. Water was doubly distilled before use.

**Preparation of FP–ANI and FP–PANI Gels.** A stock of anilinium chloride solution was prepared by dissolving 0.4 mL of aniline in 20 mL of 0.2 N HCl. FP (10 mg) was dissolved in 2 mL of dilute NaHCO<sub>3</sub> (~1 mg/mL) solution by mild heating, and then 1 mL of the anilinium chloride solution was added to this solution. Formation of a white-colored FP–ANI gel was observed immediately. However, addition of 1 mL of 0.2 N HCl to the basic solution of FP formed an assembly, and no gelation was observed. The FP–ANI gel thus obtained was metastable, and upon aging, it gradually broke down (after ca. 4 h). The molar ratio of ANI to FP used in most of the work was 7:1, and the gel formed is termed FP–ANI gel in this article.

Five milliliters of an aqueous solution of ammonium persulfate [APS, (NH<sub>4</sub>)<sub>2</sub>S<sub>2</sub>O<sub>8</sub>, 114 mg, 0.5 mmol] was added to the FP–ANI gel, and the mixture was kept undisturbed at 30 °C for 24 h to accomplish the polymerization of aniline inside the gel matrix. A prominent color change of the gel from white to deep green was observed (Figure S1, Supporting Information). The FP–PANI gel was washed repeatedly with water to remove APS and oligoaniline. The FP–PANI gel did not show any sign of breakage during the course of polymerization, and it was stable for weeks. To determine the effect of PANI on the mechanical properties of the gels, we prepared more sets of gels having different ANI/FP molar ratios and subsequently polymerized them with required quantity of APS for 24 h at 30 °C.

**Microscopy.** The morphologies of the assembly and the gels were investigated by transmission electron microscopy (TEM). Small portions of the FP assembly, FP–ANI gel, and FP–PANI gels were diluted and drop-casted on carbon-coated copper grid (300 mesh), and the samples were dried in open air at 30 °C. Finally, the samples were kept in a vacuum overnight before analysis.

**Spectroscopy.** The UV–vis spectra of the FP solution, diluted FP–ANI gel, and an aqueous dispersion of the FP–PANI gel were recorded with a Hewlett-Packard UV–vis spectrophotometer (model 8453) in a cuvette of 0.1-cm path length. A fluorescence study of the FP solution and the FP–ANI and FP–PANI gels was carried out in a Horiba Jobin Yvon Fluoromax 3 instrument. Each gel sample was prepared in a quartz cell of 1-cm path length and was excited at 280 nm. The emission scans were recorded from 300 to 600 nm using a slit width of 5 nm with a 1-nm wavelength increment and an integration time of 0.1 s. The FTIR spectra of pure components and the xerogels were recorded using KBr pellets in a PerkinElmer FTIR instrument (FT-IR-8400S).

**Diffraction Study.** Wide-angle X-ray scattering (WAXS) experiments on pure FP and FP–ANI and FP–PANI xerogels were performed with a Bruker AXS diffractometer (model D8 Advance) using a Lynx Eye detector. The instrument was operated at a 40 kV voltage and a 40 mA current. Samples were placed on glass slides and were scanned in the range of  $2\theta = 1$ –40° at a scan rate of 0.5 s/step with a step width of 0.02°.

**Rheology.** To understand the mechanical properties of the gels, rheological experiments were performed with an advanced rheometer (AR 2000, TA Instruments, New Castle, DE) using a cone–plate geometry on a Peltier plate. The diameter of the plate was 40 mm, and the cone angle was 4° with a plate gap of 121  $\mu$ m.

**Conductivity.** The dc conductivity of the dried gel samples was measured by the two-probe method at 30 °C with an electrometer (Keithley, model 617). The conductivity was measured by taking the samples between two indium–titanium

oxide (ITO) conducting strips of 1-mm width placed perpendicularly. The area of the sample was  $0.01\text{ cm}^2$ , and a screw gauge was used to measure the thickness ( $d$ ) of the samples. The conductivities of the sandwiched samples were measured by an electrometer (Keithley, model 617) at  $30\text{ }^\circ\text{C}$  using the equation

$$\sigma = \frac{1}{R} \frac{d}{a}$$

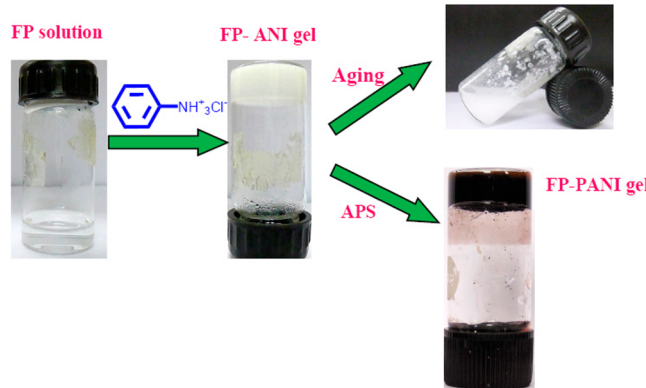
where  $R$  is the resistance of the sample obtained from the electrometer and  $a$  is the area of the electrode. The current–voltage ( $I$ – $V$ ) characteristics of the xerogels were measured by taking the samples between two indium–titanium oxide (ITO) conducting strips of 1-mm width placed perpendicularly.<sup>43</sup> The  $I$ – $V$  characteristics were recorded by (i) scanning from 0 to +5 V, (ii) scanning from +5 to –5 V, and then (iii) performing a reverse scan from –5 to 0 V. The  $I$ – $V$  characteristics under light illumination were studied separately by illumination with a light of 1 sun using a solar simulator (Newport Corp., Irvine, CA; model no. 67005).

**Impedance Spectroscopy.** For impedance measurements, we used a Solarton SI 1260 impedance analyzer (Soltarion, London, U.K.). Here, the xerogels were sandwiched between two indium–titanium oxide (ITO) conducting strips of 1-mm width placed perpendicularly, and the ITO strips were connected through connecting wires to the impedance meter using Ag paste. Here, ITO strips were used as electrodes, and Ag paste was used to connect the wires to the ITO electrodes. The impedance measurements of the xerogels were carried at  $30\text{ }^\circ\text{C}$  over the frequency range from 1 to  $10^7\text{ Hz}$ . The ac perturbation was 100 mV at 0 V dc level. In the Nyquist plot, the imaginary part of impedance ( $Z''$ ) was plotted on the  $+Y$  axis, and the real part ( $Z'$ ) was plotted on the  $X$  axis, representing a typical Cole–Cole plot in the complex impedance plane.

## RESULTS AND DISCUSSION

A coassembled gel of aniline with FP was prepared by the addition of anilinium chloride to a basic solution of FP. Gel formation occurred instantly and was characterized by the cessation of flow in the test tube inversion experiment. The FP–ANI gel thus obtained was metastable, as it gradually broke down upon aging for  $\sim 4\text{ h}$  (Scheme 2). Upon addition of ammonium persulfate (APS) solution, the FP–ANI gel became

**Scheme 2. Instant Formation of FP–ANI gel by the Addition of Anilinium Chloride to a Basic Solution of FP, Its Metastability, and the Formation of FP–PANI Gel**



polymerized, producing a dark green-colored FP–PANI gel. It is very interesting to note that the polymerization of aniline induced stability in the gel matrix as the gel did not break down during the course of polymerization (24 h). The FP–PANI gel was stable for weeks, and it also exhibited better mechanical properties than the FP–ANI gel.

**Structural Analysis.** To obtain a proper understanding of the mechanism of gel formation of the FP–ANI and FP–PANI gels, it is important to gain an insight into the structure of the complexes. The FTIR spectrum of pure FP (Figure 1) exhibits

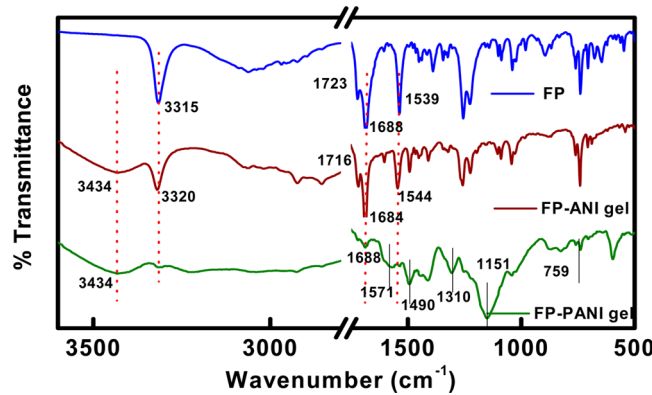


**Figure 1.** FTIR spectra of FP powder and FP–ANI and FP–PANI xerogels.

two  $>\text{C=O}$  stretching peaks at  $1723$  and  $1688\text{ cm}^{-1}$  for the acid and amide carbonyl groups, respectively. In the spectrum of the FP–ANI gel, both of these peaks shift to lower frequencies ( $1716$  and  $1684\text{ cm}^{-1}$ , respectively), which might be due to the formation of strong H-bonding interactions between FP and aniline. In the spectrum of the FP–PANI gel, the carbonyl stretching peak of the  $-\text{COOH}$  group has shifted to  $1720\text{ cm}^{-1}$  with diminished intensity. This smaller blue shift of the  $>\text{C=O}$  vibration peak compared to that in the FP–ANI gel suggests that the H-bonding interaction is not as strong as with the monomers (anilinium ion) because the covalent linkage in the PANI chain might impede the H-bonding process probably as a result of conformational rigidity. The vibration peak of the amide carbonyl group ( $1684\text{ cm}^{-1}$ ) is also blue-shifted by  $4\text{ cm}^{-1}$  for the same reason. At  $1544\text{ cm}^{-1}$ , the carboxylate ion ( $-\text{COO}^-$ ) vibration peak of FP coincides with the  $-\text{NH}$  bending vibration of the amide group in the FP–ANI gel. This peak almost vanishes in the FP–PANI gel, and a probable reason might be that the acidity developed during the polymerization of ANI might cause the formation of undissociated carboxylic acid group.<sup>44</sup> The spectra of FP–ANI and FP–PANI gels exhibit a broad peak at  $3433\text{ cm}^{-1}$ , indicating the presence of a strong hydrogen-bonding interactions between the  $-\text{NH}$  groups of aniline and polyaniline and the  $-\text{COOH}$  groups of FP molecules. The  $-\text{NH}$  stretching vibration frequency of the amide group of FP at  $3315\text{ cm}^{-1}$  shifts to  $3320\text{ cm}^{-1}$  in the FP–ANI gel, probably indicating the breakage of the stronger intramolecular H-bonds of FP during coassembly.<sup>39</sup> Typical stretching bands at  $759$ ,  $1151$ ,  $1310$ ,  $1490$ , and  $1571\text{ cm}^{-1}$  for the FP–PANI gel indicate the formation of polyaniline, as the  $1571$  and  $1490\text{ cm}^{-1}$  peaks correspond to the benzonoid (B) and quinonoid (Q) rings of PANI, respectively; the  $1151\text{ cm}^{-1}$  peak is for the doped quinonoid structure ( $\text{Q}=\text{N}^+\text{H}-\text{B}$  or  $\text{B}-\text{N}^+\text{H}-\text{B}$ ) due to the

formation of a polaronic structure and  $1310\text{ cm}^{-1}$  is for C—N stretching of secondary amine.<sup>45–47</sup>

To monitor the structural changes during the formation of FP-ANI gel and its polymerization, powder X-ray diffraction (XRD) was performed for FP powder and FP-ANI and FP-PANI xerogels. It is evident from the results in Figure 2 that the

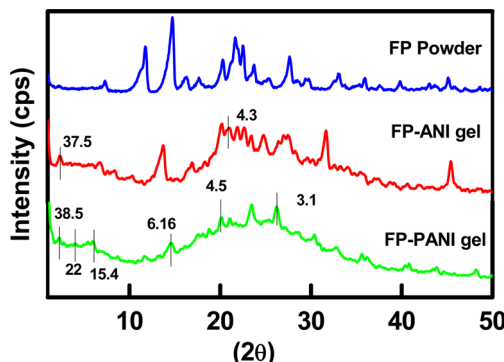


**Figure 2.** XRD patterns of pure FP powder and FP-ANI and FP-PANI xerogels.

crystalline structures of FP-ANI and FP-PANI xerogels are different from each other and also from that of the FP powder. The crystalline peaks of FP powder disappear, and new crystalline peaks appear in the diffractogram of FP-ANI xerogel, indicating the formation of a new crystalline structure. Diffraction peak at  $2\theta = 2.35^\circ$  ( $d = 37.5\text{ \AA}$ ) might arise because of the long-range order, and the peak at  $2\theta = 20.9^\circ$  ( $d = 4.3\text{ \AA}$ ) characterizes the  $\pi-\pi$  stacking distances between the aniline units of the FP-ANI system. The diffractogram of the FP-PANI xerogel exhibits the characteristic peaks of PAN at  $2\theta = 6.0^\circ$  ( $d = 15.4\text{ \AA}$ ),  $20.2^\circ$  ( $d = 4.5\text{ \AA}$ ), and  $26.2^\circ$  ( $d = 3.1\text{ \AA}$ ). The peak centered at  $2\theta = 6^\circ$  is associated with the periodicity arising from the association of FP and PANI, and the peak centered at  $2\theta = 20.2^\circ$  is attributed to the periodicity in the direction parallel to the polymer chain, whereas the peak at  $2\theta$

$= 26.2^\circ$  is due to the periodicity in the direction perpendicular to the polymer chain arising from the  $\pi$ -stacking process.<sup>48</sup> From the diffractogram of the FP-PANI gel, it is apparent that the peak at lower angle ( $2\theta = 2.29^\circ$ ) might arise from the lamellar structure with a lamellar thickness of  $38.5\text{ \AA}$ , indicating that the lamellar structure of FP-ANI is not disturbed by polymerization.<sup>45</sup> Also, it is important to note that there is a peak at  $2\theta = 4^\circ$  having a  $d$  spacing of  $22\text{ \AA}$  that might arise from the supramolecular structure, and a careful analysis can recognize an additional nascent peak ( $2\theta \approx 23.5^\circ$ ) with a  $d$  spacing of  $3.78\text{ \AA}$  arising from the  $\pi$ -stacking of the chains.

We performed the energy minimization of the FP-ANI complex using density functional theory (DFT) calculations to interpret the above XRD data (Figure 3a,b). The diffraction peak characterizing  $d = 4.3\text{ \AA}$  matches well with the  $\pi-\pi$  stacking distance between the supramolecularly attached aniline units obtained from the DFT calculations. The enlarged diffractogram of the FP-ANI gel in the range of  $2\theta = 3.0\text{--}6.0^\circ$  (Figure S2, Supporting Information) exhibits a peak at  $2\theta = 5.5^\circ$  having a  $d$ -spacing value of  $16\text{ \AA}$ , which nearly equals the energy-minimized distance of  $17.68\text{ \AA}$  for FP-ANI xerogel (Figure 3a) at a 1:1 molar composition. The peak at  $3.4^\circ$  ( $d = 26.1\text{ \AA}$ ) corresponds to the formation of a complex in which two FP-ANI units are connected by  $\pi-\pi$  stacking between the aniline molecules (Figure 3b). Considering an additive approximation of the repeating distances, it might be reasonable to think that, upon  $\pi$ -stacking, the length of a  $\pi$ -stacked FP-ANI system is  $(28.2 - 17.7) = 10.5\text{ \AA}$  and, hence, the repeat distance with the third FP-ANI unit is  $(28.2 + 10.5) = 38.7\text{ \AA}$ , which corresponds to the XRD peak at  $2\theta = 2.35^\circ$  ( $d$  spacing =  $37.5\text{ \AA}$ ; not shown at Figure 3). Thus, the model clearly explains the XRD data of the FP-ANI system, indicating the growth of the supramolecular complex formed (evident from the nonbonding distance of  $1.76\text{ \AA}$ ) by  $\pi-\pi$  stacking as is evident from the  $\pi-\pi$  stacked distance of  $4.3\text{ \AA}$ . However, we were unable to draw the energy-minimized structure of the FP-PANI system because of the large dimensions of the PANI chains.

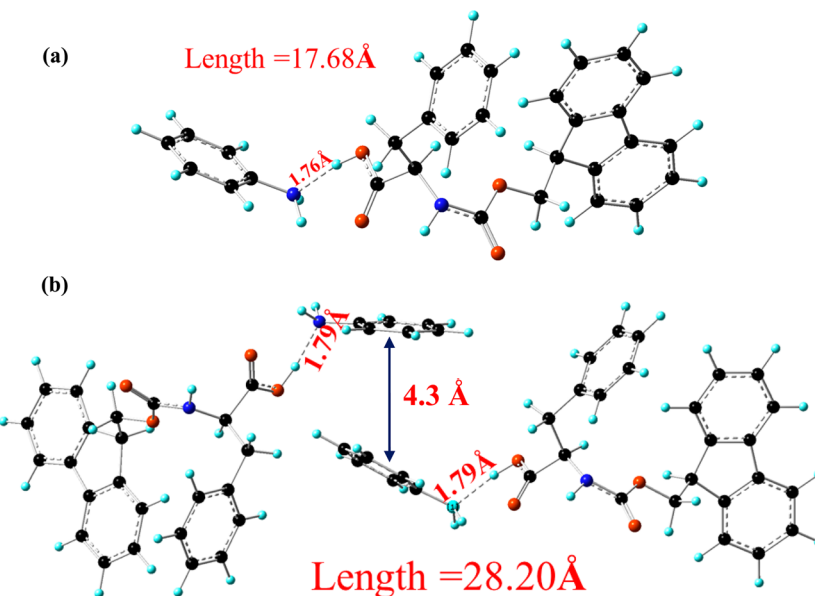


**Figure 3.** Energy-minimized structures of (a) one FP-ANI unit and (b) a complex of two FP-ANI units by  $\pi$  stacking between aniline molecules obtained from the DFT program.

**Morphology.** Transmission electron microscopy (TEM) was carried out to investigate the morphology of FP-ANI and FP-PANI gels. Figure 4a,b presents TEM images of FP-ANI

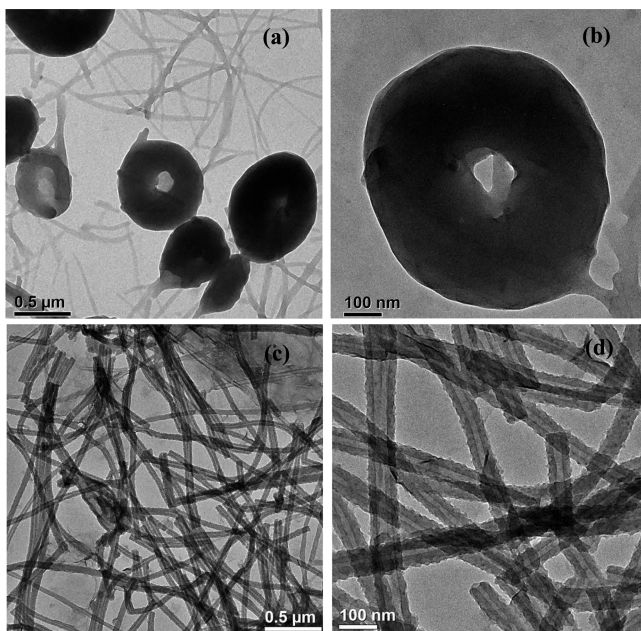
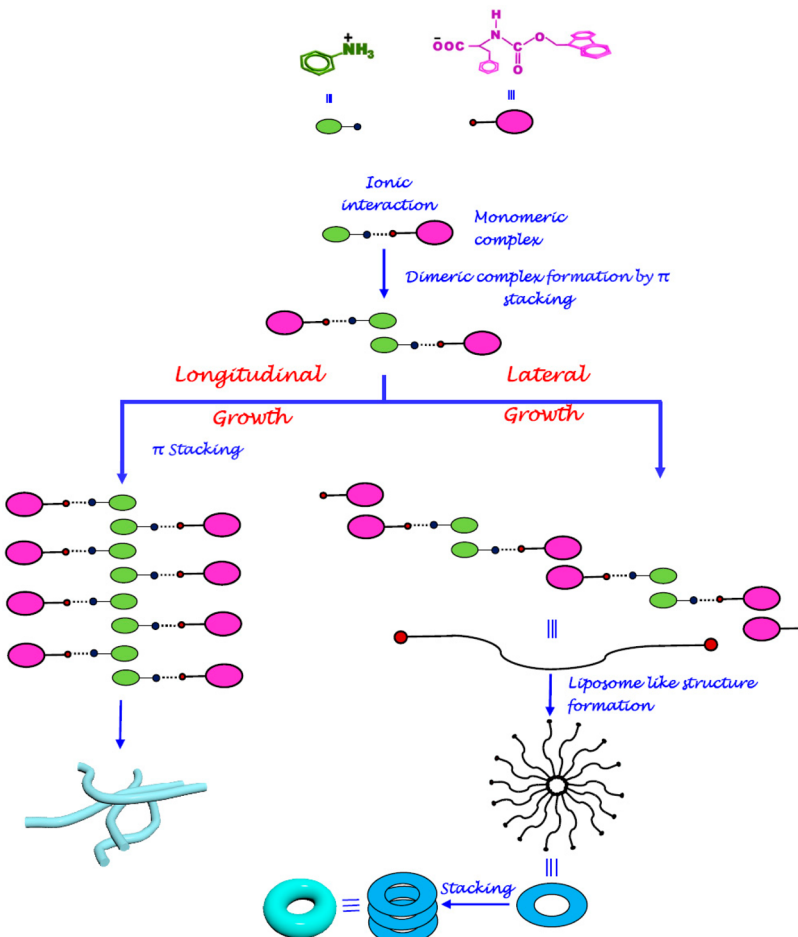


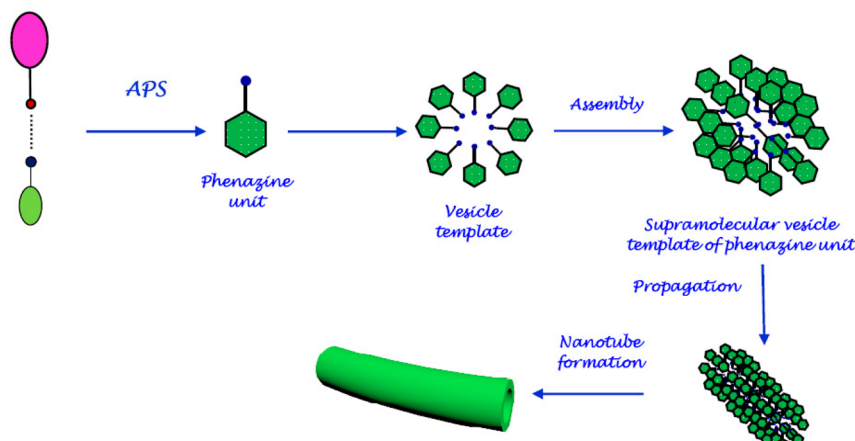
Figure 4. TEM images of (a,b) FP-ANI and (c,d) FP-PANI xerogels.

gel, and it is evident from the images that FP-ANI gel exhibits a morphology consisting of a mixture of fibers and doughnuts. However, the self-assembly of FP obtained by acidifying the basic solution of FP with diluted HCl exhibits only a rodlike morphology (Figure S3, Supporting Information). Here, nucleation of FP crystallites commences, producing rods of FP crystals. In contrast, in the case of the FP-ANI system, the supramolecular organization of the two components produces the doughnut and fibrous structure. Scheme 3 presents a probable model of supramolecular organization of the components through ionic interactions between anionic FP and the anilinium ions produced by doping. The supramolecular FP-ANI complex can grow laterally by consecutive  $\pi$ -stacking followed by ionic interaction, and the longitudinal growth occurs only though  $\pi$ -stacking processes between the respective  $\pi$ -clouds of the components. Depending on the relative magnitude of competition between the longitudinal and lateral growth processes, the formation of doughnuts and fibers can be explained as follows:

During doughnut formation, the lateral growth occurs very rapidly to a maximum extent until the ionic density at the surface of both ends is very large, preventing further progress of the lateral  $\pi$ -stacking process. Because of the increase in the supramolecular length, the charged surfaces at both ends tends to self-organize into a liposome-like structure. The interior of structure therefore entraps the solvent water, and the outer surface of the structure, because of its larger ionic density, also

Scheme 3. Schematic Model Explaining Fiber and Doughnut Formation in FP-ANI Supramolecular Gel



Scheme 4. Schematic Model Showing the Formation of FP-PANI Nanotubes<sup>a</sup>

<sup>a</sup>FP molecules are not shown in model for clarity.

attracts water dipoles. The surface force at the outer surface of the doughnuts helps entrap the solvent water, and thus, at both the inner and outer surfaces of the doughnuts, water molecules become trapped, producing the gel. The average outer diameter of the doughnuts is  $720 \pm 160$  nm, the average inner diameter is  $111 \pm 12$  nm, and the average cell thickness is  $\sim 300$  nm. Considering the energy-minimized length (17.7 Å) of a monomeric complex of FP and ANI, it can be surmised that  $\sim 200$  such monomeric units assemble to produce the doughnut morphology. The doughnut morphology is therefore composed of stacked liposomes (Scheme 3) describing the above scheme of doughnut formation. Small fractions of fibers are also present in the FP-ANI gel that can be attributed to the predominance of longitudinal growth over the lateral growth of the FP-ANI complex. The average diameter of the fibers was found to be  $31.5 \pm 1.8$  nm, and it might be reasonable to conclude from the data that about 20 such  $\pi$ -stacked FP-ANI supramolecular complexes can self-assemble to produce the fiber cross section (for simplicity, only two FP-ANI complexes are shown in Scheme 3), which grows through longitudinal  $\pi$ -stacking to produce the long fiber. The reason for the metastability of FP-ANI gel is yet unknown, and it might be due to the strong competition between the two types of growth (lateral and longitudinal), which might even exist in the gel state during annealing at room temperature (30 °C), causing a disorganized structure and thus breaking the gel.

Addition of APS solution to the FP-ANI gel initiates the polymerization of aniline monomers anchored to the FP molecules to generate the FP-PANI gel, which exhibits a nanotubular morphology (Figure 4c,d). Visualization of a clear contrast between the edges and the central part of the nanostructures in the TEM images indicates the formation of nanotubes with an average outer diameter of  $61 \pm 6$  nm and an inner diameter of  $19.6 \pm 8$  nm. The nanotubes consist of a supramolecular complex of both FP and polyaniline (PANI) where the ionic ends remain at both the inner and outer parts because of their greater hydrophilicity and the nonpolar parts of the FP-PANI complex remain at the interior because of its hydrophobicity. The formation mechanism of PANI nanotubes can be understood using the explanation reported by Stejskal et al.<sup>49</sup> The aniline oligomers (phenazine) are produced during the first stage of aniline oxidation, and they act as templates for the adsorption of N-phenylphenazines produced in solution

during the induction period. This causes the formation of vesicular template where the polar group of FP-PANI remains at the inner surface and the short N-phenylphenazines are stacked around the phenazine nanocrystallites. Thus, it acts as a template for nanotubular growth, and the PANI chains then grow from the stacked N-phenylphenazine initiation centers, producing the walls of nanotubes as presented in Scheme 4.

**Optical Properties.** Figure S4a (Supporting Information) presents the UV-vis spectra of the solution of FP-PANI gel. The band at 280 nm can be ascribed to the  $\pi-\pi^*$  transition in the benzenoid rings of the PANI chains. The 443 nm band might originate from the transition from the polaron band to the  $\pi^*$  band of the PANI chain.<sup>45</sup> A dominant band at around 845 nm represents the  $\pi$ -band-polaron-band transition of doped PANI chains. These results undoubtedly indicate the formation of the emeraldine salt form of PANI in the FP-PANI gel.<sup>50</sup> In the inset of the figure are presented the absorption spectra of FP and FP-ANI solutions, where the absorption peaks at 264 and 280 nm originate from the  $\pi-\pi^*$  transition of both systems and, in the case of FP-ANI, the red shift from that of FP can be attributed to the supramolecular complex formation.

It is known that FP exhibits fluorescence; however, neither ANI nor PANI has fluorescence properties. Therefore, it would be interesting to examine the fluorescence properties of FP in the above gels. The photoluminescence spectra of FP solution and FP-ANI and FP-PANI gels are presented in Figure S4b (Supporting Information) for the same concentration of FP. It is apparent from the figure that the emission peak of FP (407 nm) shows a red shift of 33 nm in the FP-ANI gel and that the peaks becomes broader with a 33% increase of fluorescence intensity. The red shift and increase of the broadness of the emission peak can be attributed to the stabilization of excitons in the FP-ANI supramolecular complex. Also, the increase in intensity can be attributed to the gel structure, where the hydrophobic core structure formation in the gel prohibits the decay of excitons with the solvent molecules. It is interesting to note that, in the FP-PANI gel, the fluorescence intensity was completely diminished because of the good quenching ability of PANI chains.

**Mechanical Properties.** Gels are semisolid materials with inherent properties of storage and dissipation of energy. The storage modulus ( $G'$ ) signifies the amount of energy stored in

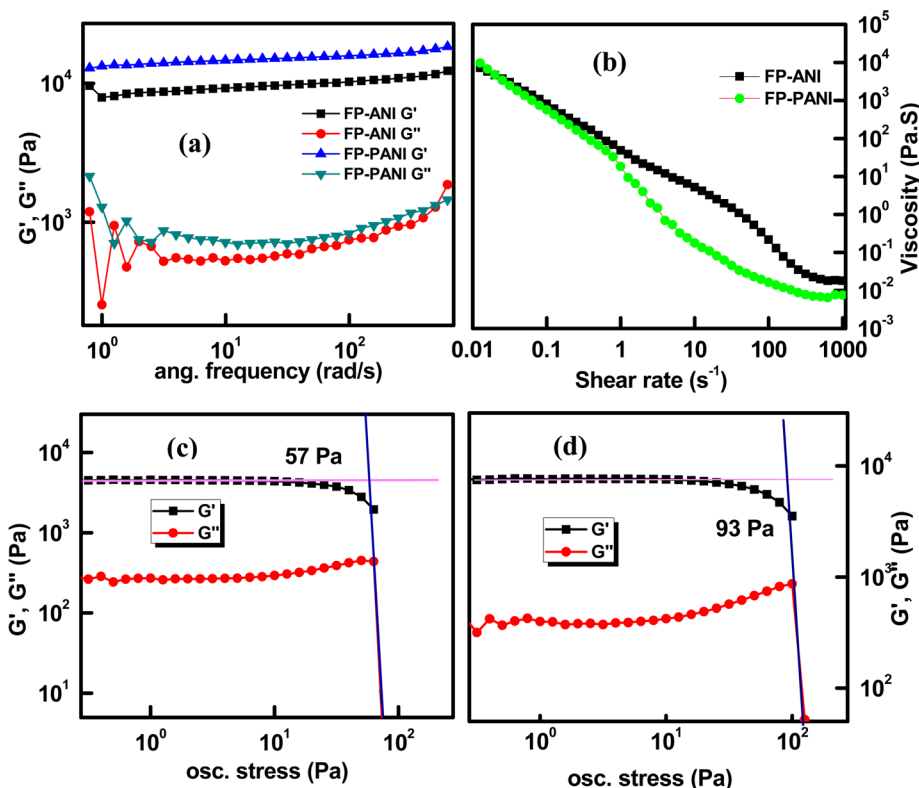


**Figure 5.** (a) Frequency-dependent oscillatory rheology of the gels and (b) shear viscosity vs shear rate plot of FP-ANI and FP-PANI gels at 25 °C. (c,d) Stress dependency of storage and loss modulus of (c) FP-ANI and (d) FP-PANI gel at a frequency of 1 Hz.

the system, and the loss modulus ( $G''$ ) designates the amount of energy dissipated within the system upon the application of frequency. In the gel phase  $G' > G''$  and  $G'(\omega) \approx \omega^0$ , where  $\omega$  is the angular frequency. As the FP-ANI gel is metastable in nature, its rheological properties were measured prior to breakage (after 1 h of gel formation). The dynamic frequency sweep experiments of FP-ANI and FP-PANI gels are depicted in Figure 5a. It is obvious from the figure that both of the gels show a wide viscoelastic region. Also, in both cases, the storage modulus ( $G'$ ) is considerably higher than  $G''$ , which confirms the gel nature of the samples. It is interesting to note that both the  $G'$  and  $G''$  values of the FP-PANI gel are higher than those of the FP-ANI gel. This indicates that polymerization of aniline not only confers stability on the metastable FP-ANI gel but also induces improved mechanical properties. The excellent increase of the storage modulus (61%) of the FP-PANI gel can be attributed to the formation of chemical bonds between the ANI units and the formation of a nanotube structure; both facilitate the storing of energy, increasing the storage modulus. The same reason can also explain the increase in the loss modulus of the FP-PANI gel. To comprehend the effect of PANI on the mechanical properties of the gels, we also performed frequency sweep experiments on varying concentrations of aniline in the gels after polymerization. It was observed that the value of  $G'$  for the PANI gels increased with increasing aniline concentration, and it reached its maximum value when the ANI/FP molar ratio was equal to 7 (Figure S5, Supporting Information) (designated as the FP-PANI gel in the whole article), indicating that gel strength increases with increment of aniline with a maximum at a molar ratio of AN/FP = 7:1. At higher ANI concentrations, probably all of the PANI chains do not take part in the coassembly process,

causing a decrease of  $G'$ . Figure 5b depicts the shear viscosity versus shear rate plot of the FP-ANI and FP-PANI gels. Both gels exhibit shear-thinning behavior that can be ascribed to shear-induced breaking of the gels. However, it is very interesting to observe that, at very low shear rates ( $0.01 s^{-1}$ ), the viscosity of the FP-PANI gel is higher (9007 Pa·s) than that of the FP-ANI gel (7262 Pa·s). However, above a shear rate of  $0.02 s^{-1}$ , the viscosity of the FP-ANI gel crosses the value for the FP-PANI gel and remains higher than that of the FP-PANI gel for the rest of the shear rate values. The higher value of viscosity of the FP-PANI gel at low shear rate might be due to the formation of covalent polymers forming entangled networks. At higher values of shear rate, those entanglements are disrupted by the imposed deformation, and hence, the cross-link density of the network becomes depleted, thereby causing the higher rate of shear thinning compared to that of the FP-ANI gel. The shear thinning of FP-ANI gel can be attributed to the gradual disruption of the supramolecular organization with increased applied shear. Figure 5c,d shows the stress dependency of the storage and loss moduli of the gels. FP-ANI gel breaks at an oscillator stress of 57 Pa, and the FP-PANI gel breaks at an oscillator stress of 93 Pa, indicating the higher stability of the FP-PANI gel because of the covalent nature of PANI and easy dissipation of stress by the nanotubular superstructure.

Viscoelasticity is the property of materials that display both viscous and elastic characteristics while undergoing deformation. Viscous materials oppose shear flow and strain linearly with time when a stress is applied, whereas elastic materials undergo strain on applied stress and rapidly return to their original state once the stress is removed. Viscoelastic materials combine both of these properties and exhibit time-dependent

strain.<sup>51</sup> FP-PANI gel shows evidence of viscoelastic properties, as established from creep recovery experiments (Figure 6).

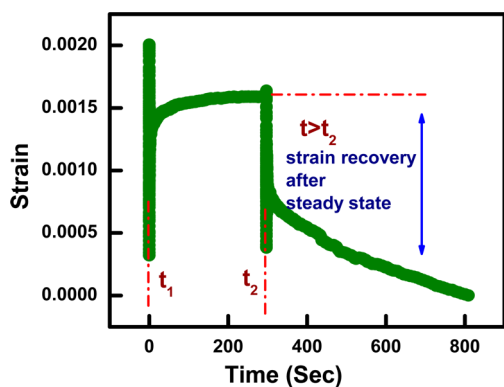


**Figure 6.** Stress relaxation as a function of time in the creep recovery investigated with FP-PANI gel at an applied stress of 0.5 Pa.

In the creep phase, the strain curve displays a jump in strain value in response to an applied stress of 0.5 Pa, which might be due to a pure elastic nature; then, a subsequent time-dependent small increase in strain occurs, and finally, the strain becomes almost nonvariant.<sup>52</sup> After removal of the stress from the FP-PANI gel ( $t > t_2$ ), the material shows an initial strain recovery to almost negligible strain value and then a gradual decrease in strain from the original value with increasing aging time. No definite reason for this phenomenon is known to us, and probably, a secondary structure of PANI is produced, causing strain-induced crystallization that gradually squeezes, eradicating solvent from the matrix of the gel. Hence, it can be concluded that the FP-PANI gel exhibits a considerable viscoelastic nature in the recovery zone.

**Electrical Properties.** The dc conductivities of the dried FP-ANI and FP-PANI gels are  $9.4 \times 10^{-9}$  and  $1.2 \times 10^{-2}$  S·cm<sup>-1</sup> respectively. This huge increase in conductivity in the latter sample compared to the former is probably due to the formation of the emeraldine salt form of PANI, as evidenced by the UV-vis spectra (Figure S4a, Supporting Information), producing a conjugated chain that facilitates the easier movement of charge carriers. Radical cations (polarons) are formed because of the doping of PANI by FP through an acid–base-type interaction due to coassembly. The polarons (evident from UV-vis spectroscopy) easily move from one end of the polymer chain to the other through the extended  $\pi$ -orbital system, which helps improve the dc conductivity value. The conductivity of the FP-PANI xerogel is 2 orders higher than that of the pure PANI nanotubes ( $7.8 \times 10^{-4}$  S·cm<sup>-1</sup>),<sup>53</sup> and this increase in conductivity can be attributed to the  $\pi$ -stacking of the FP-PANI complex facilitating charge delocalization through the  $\pi$ -stacked complex and causing easier charge movement. The current–voltage ( $I$ – $V$ ) curves of the FP-ANI xerogel (Figure 7a) exhibit a hysteresis behavior probably because of the presence of some space charges trapped in the FP-ANI complex facilitating more current flow in the forward bias than in the backward bias. The  $I$ – $V$  nature of the FP-PANI xerogel (Figure 7b) resembles the behavior of a semiconductor–metal junction;<sup>54</sup> therefore, it behaves as a semiconductor with a small density of states in the band gap, probably because of the introduction of narrow polaron and bipolaron bands within the band gap. From Figure 7b, it is also evident that the FP-PANI xerogel generates a much higher

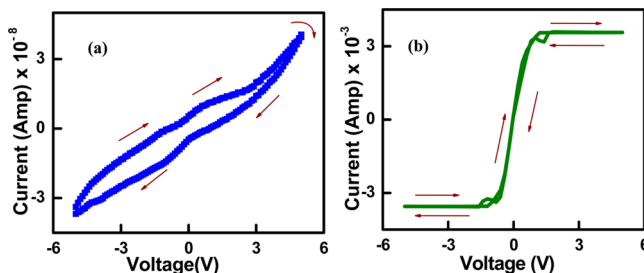


**Figure 7.**  $I$ – $V$  characteristic curves of (a) FP-ANI and (b) FP-PANI xerogel measured at 30 °C.

amount of current than the FP-ANI xerogel, which can be attributed to the formation of interstate polaronic/bipolaronic bands making the interband distance small enough to help the holes move around quite freely upon application of a bias voltage.

Polyaniline acts as a donor, and FP, because of its Fmoc group, can act as a weak acceptor, so there is a possibility of photoconductivity in the FP-PANI xerogel.<sup>53</sup> It is apparent from the  $I$ – $V$  plots under both dark and illuminated conditions (Figure 8a) that the FP-PANI xerogel exhibits a higher current

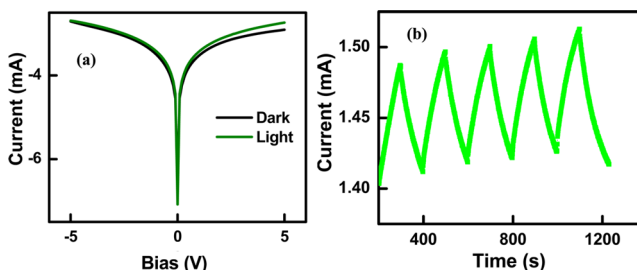


**Figure 8.** (a) Logarithmic  $I$ – $V$  curve of the FP-PANI xerogel under different conditions. (b) Photoresponse cycle turned “on” and “off” by switching the white light illumination on and off, respectively.

under illuminated conditions than under dark conditions at both positive and negative bias voltage. It is to be noted here that the photocurrent at positive bias is somewhat higher than that at negative bias. The photoresponse property of the material was further investigated by recording the photocurrent growth (for 100 s) and decay (for 100 s) at a time gap of 1 ms for a bias voltage of +5 V with white light illumination (Figure 8b). The results demonstrate several such photocurrent cycles, indicating that the material can be reversibly turned on and off under illuminated and dark conditions, respectively. The increment of current after white light irradiation is  $\sim 0.1$  mA, whereas pure PANI nanotubes exhibit a photocurrent increment of  $\sim 0.03$  mA.<sup>53</sup> The data are reproducible as observed from the different cycles after a fixed time interval of 100 s. Also, it is important to note that the material does not degrade under illuminated conditions. After irradiation with light, the absorption of energy can create electron–hole pairs that separate to a lower extent in the electric field, and this is responsible for creating a low value of the photocurrent in the FP-PANI nanotubes.<sup>55</sup> The low rate of increase of the photocurrent and its slow decay after switching off light can be explained in terms of the structure of the coassembled gel. Here, the doped PANI acts as a donor, and upon irradiation, the photoelectron is accepted by the acceptor FP. Because of  $\pi$ – $\pi$  stacking of the phenyl ring of FP and the aniline moieties

of PANI, a resonance stabilization of the photoelectron takes place before it enters the conduction band of the hybrid. When the irradiation is stopped, the photoelectron then comes down from the conduction band to the ground state in the same path through resonance stabilization and takes a longer time than in the forward process.

ac impedance spectroscopy is widely used as a nondestructive testing method for the study of electrolytic materials such as ceramics and polymer electrolytes.<sup>56,57</sup> In Figure 9, Nyquist

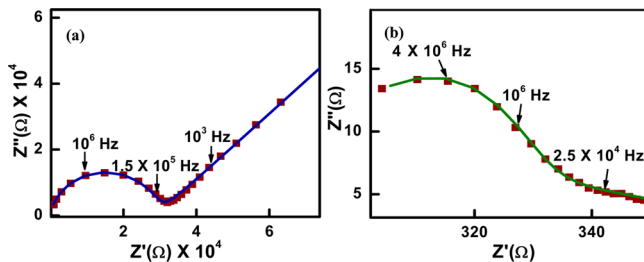


Figure 9. Nyquist plots for (a) FP-ANI and (b) FP-PANI xerogels.

plots for the FP-ANI and FP-PANI xerogels are presented. The impedance diagrams are typically interpreted based on equivalent circuit models that can unambiguously elucidate the electronic properties of the materials. The Nyquist plot of FP-ANI xerogel (Figure 9a) was fitted based on a modified Randles equivalent circuit consisting of a constant phase element (CPE) and a Faradaic impedance in parallel. The Faradaic impedance is a combination of a charge-transfer resistance ( $R_{ct}$ ) and a Warburg impedance ( $Z_w$ ). The Warburg element is a frequency-dependent element whose impedance is mathematically determined by the equation

$$Z_w = \frac{C}{\sqrt{\omega}} - j \frac{C}{\sqrt{\omega}} \quad (1)$$

where  $C$  is the Warburg constant and  $\omega$  is the angular frequency. A CPE is also a frequency-dependent element that is calculated as

$$Z_{CPE} = \frac{1}{A(j\omega)^n} \quad (2)$$

where  $A$  and  $n$  are constants.  $n$  can have values ranging between 0 and 1, and when  $n = 1$ , the CPE reduces to a capacitance.<sup>58</sup> This type of nonideal capacitive behavior in the FP-ANI xerogel can be attributed to inhomogeneous conductivity or charge trapping, which is also evident from the  $I-V$  characteristics (Figure 7a). The Nyquist plot of the FP-PANI xerogel (Figure 9b) is different from that of the FP-ANI xerogel, and it exhibits almost a semicircle, indicating the existence of both resistive ( $R$ ) and capacitive ( $C$ ) features in the xerogel material connected in a parallel mode.<sup>59-61</sup> To interpret the plot of Figure 9a,b, equivalent circuit models were made as shown in Figure 10. We fitted the impedance curves with a Z-view program (Solartron, London, U.K.), and the resistance and capacitance values were calculated. For the FP-ANI xerogel, the charge-transfer resistance ( $R_{ct}$ ) and CPE values were calculated to be  $29 \text{ k}\Omega$  ( $\pm 0.10 \text{ k}\Omega$ ) and  $0.02 \text{ nF}$  ( $\pm 0.001 \text{ nF}$ ), respectively, whereas the Warburg impedance ( $Z_w$ ) was  $487 \text{ k}\Omega$  ( $\pm 0.10 \text{ k}\Omega$ ). For the FP-PANI xerogel, the resistance values were found to be  $R_1 = 246.2 \text{ }\Omega$  ( $\pm 1 \text{ }\Omega$ ) and  $R_2 = 70.5 \text{ }\Omega$  ( $\pm 1 \text{ }\Omega$ ), and the value for the CPE was  $12 \text{ mF}$  ( $\pm 0.1 \text{ mF}$ ). It is noteworthy that the polymerization of aniline stimulated a

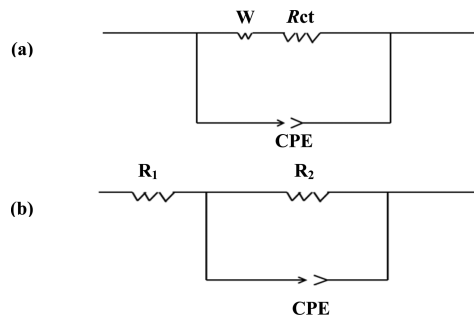
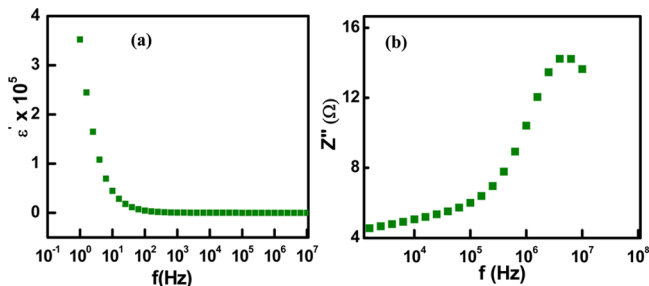


Figure 10. Equivalent R-C circuits of (a) FP-ANI and (b) FP-PANI xerogels.

significant decrease in resistance with a dramatic increase in capacitance in the FP-PANI xerogel compared to its precursor. The most probable reason might be the supramolecular interactions between the FP and PANI chains, which increase the charge storage in the matrix through partial delocalization. In the impedance spectra of the FP-ANI xerogel, both a semicircle at high frequency and a spike at low frequency were observed (Figure 9a). The semicircle at high frequencies occurs because of the bulk resistance, and the spike at low frequencies corresponding to the Warburg impedance is due to the semi-infinite diffusion of ions at the electrode.<sup>62</sup> The appearance of the spike in this system indicates that the conduction is ionic in nature. However, in the impedance spectra of the FP-PANI xerogel, the spike is absent, indicating that the contribution is mainly from the bulk and no contribution from ionic conductivity exists.

There is a good possibility that the difference in morphology of the FP-ANI and FP-PANI xerogels can influence the impedance property of the materials. FP-ANI exhibits a mixture of fiber- and doughnut-type morphologies. However, the FP-PANI gel exhibits a nanotubular morphology. In impedance, mainly two properties of the system, namely, resistance and capacitance, are manifested. The long nanotubes of FP-PANI have a greater possibility of charge storage for a unit increase in voltage than the doughnuts in the FP-ANI gel because of the large inner and upper surface areas of the nanotube. This dramatically increases the capacitance values. The  $\sim 2000$ -times higher resistance value in FP-ANI gel compared to FP-PANI gel might be due to the two reasons: (i) the absence of conjugation as present in the PANI chain and (ii) the influence of morphology. Here, the former contribution would definitely be prominent; however, some smaller contribution of the nanotube morphology might also be present because of the easier flow of charge through the one-dimensional path, whereas in the doughnut morphology, this is not possible. Also, because of the smaller surface area of the doughnut, the diffusion of ions occurs easily in the FP-ANI gel, causing a spike at low frequency in the Nyquist plot.<sup>62</sup> This type of diffusion is not possible in the case of the FP-PANI gel, and in the Nyquist plot of the FP-PANI gel, this type of spike is not observed.

Owing to the much lower resistance and highly doped, covalently linked PANI chains facilitating  $\pi$ -electron conjugation, as well as the higher capacitance values of the FP-PANI xerogel material, further dielectrical measurements were made. The dielectric constant ( $\epsilon'$ ) and imaginary part of the impedance ( $Z''$ ) as functions of frequency of the FP-PANI xerogel are shown in Figure 11. It is obvious from Figure 11a that the dielectric constant, which indicates the alignment of



**Figure 11.** Plots of (a) dielectric constant ( $\epsilon'$ ) and (b) imaginary part of impedance ( $Z''$ ) with frequency.

both permanent and induced dipoles, decreased (from  $3 \times 10^5$  to 0.17) with increasing frequency. One probable reason for this behavior is that the rotational motions of polar FP-PANI supramolecules might not be as fast as the change in the direction of electric field (i.e., frequency), and they cannot be commensurate with the change in the direction of the ac electric field. As a consequence, the polarization decreases, and at higher frequencies, it reaches a constant minimum value.<sup>63</sup> The spectroscopic plot of the imaginary component ( $Z''$ ) versus frequency shown in Figure 11b exhibits one Debye peak, indicating that the system is isotropic (unlike the FP-ANI system) and that the impedance response in the FP-PANI xerogel sample can be represented by an equivalent parallel resistance–capacitance (R–C) circuit, as presented above.

## CONCLUSIONS

FP-ANI produces a metastable coassembled hydrogel, but upon polymerization with ammonium persulfate, it produces a stable green-colored coassembled FP-PANI hydrogel. The coassembly is produced by supramolecular interactions between FP and ANI; however, FP-PANI hydrogel has a weaker H-bonding interaction than that of FP-ANI gel. The structures of FP powder, FP-ANI, and FP-PANI xerogels are different from each other. The FP-ANI gel exhibits a mixture of doughnut and fiber morphologies, but the FP-PANI gel exhibits a nanotubular morphology. A schematic model showing the supramolecular organization of an FP-ANI complex through successive  $\pi$ -stacking and ionic interactions is used to explain the mixed morphology of FP-ANI, whereas the nanotubular morphology is explained by the growth of vesicular structure of the polyaniline oligomers. The metastability of the FP-ANI gel is attributed to the competitive nature of longitudinal and lateral growth of the FP-ANI supramolecular complex in the gel state. The UV-vis spectrum suggests a doped state of PANI in the FP-PANI gel, and the fluorescence property of FP completely vanishes due to the quenching action of PANI in the FP-PANI gel. The storage and loss moduli ( $G'$  and  $G''$ ) of the FP-PANI gel are higher than those of the FP-ANI gel. The FP-PANI gel breaks at a higher oscillator stress than the FP-ANI gel because of the presence of covalent bonds and also the well-dispersed nanotubular morphology. Also, the FP-PANI gel exhibits good strain recovery, showing excellent viscoelastic properties. FP-PANI gels have a conductivity ( $1.2 \times 10^{-2} \text{ S}\cdot\text{cm}^{-1}$ ) that is 7 orders higher than that of FP-ANI gel because of the doped nature of PANI chains in the gel. The  $I$ – $V$  characteristic curve of FP-PANI xerogel resembles the behavior of a semiconductor–metal junction. Under white light illumination, the FP-PANI xerogel exhibits a reversible on/off cycle with a

constant photocurrent value of 0.1 mA due to the donor–acceptor nature of PANI and FP, respectively. The Nyquist plot obtained from impedance measurement of the FP-PANI xerogel is different from that of the FP-ANI xerogel, and it exhibits almost a semicircle, indicating the existence of both resistive ( $R$ ) [ $R_1 = 246.2 \Omega$  and  $R_2 = 70.5 \Omega$ ] and capacitive ( $C$ ) ( $C = 12 \text{ mF}$ ) features connected in a parallel mode. Thus, the coassembled gel of polyaniline and FP is an excellent material and could find use in soft electronics, optoelectronics, and biosensors, among others, because of the mechanically strong and conducting nature of the gel.

## ASSOCIATED CONTENT

### S Supporting Information

Digital images of gels, XRD, TEM, UV-vis, fluorescence, and rheological data. This material is available free of charge via the Internet at <http://pubs.acs.org>.

## AUTHOR INFORMATION

### Corresponding Author

\*Tel.: 913324734971. E-mail: psuakn@iacs.res.in.

### Notes

The authors declare no competing financial interest.

## ACKNOWLEDGMENTS

P.C., P.B., and S.M. acknowledge CSIR, New Delhi, India, for providing a fellowship. We also acknowledge Mr T. Paul (SSP, IACS) for helping in fitting of the impedance data and Ms S. Banerjee and Prof. S. K. Pati of JNCASR, Bangalore, for the DFT calculations. The instrumental facility from the DST-sponsored “Unit of Nanoscience at IACS” project is gratefully acknowledged.

## REFERENCES

- (1) Friggeri, A.; Feringa, B. L.; van Esch, J. H. Entrapment and Release of Quinoline Derivatives Using a Hydrogel of a Low Molecular Weight Gelator. *J. Controlled Release* **2004**, *97*, 241–248.
- (2) Tiller, J. C. Increasing the Local Concentration of Drugs by Hydrogel Formation. *Angew. Chem., Int. Ed.* **2003**, *42*, 3072–3075.
- (3) Lee, K. Y.; Mooney, D. J. Hydrogels for Tissue Engineering. *Chem. Rev.* **2001**, *101*, 1869–1879.
- (4) Ellis-Behnke, R. G.; Liang, Y.-X.; You, S.-W.; Tay, D. K. C.; Zhang, S.; So, K.-F.; Schneider, G. E. Nano Neuro Knitting: Peptide Nanofiber Scaffold for Brain Repair and Axon Regeneration with Functional Return of Vision. *Proc. Natl. Acad. Sci. U.S.A.* **2006**, *103*, 5054–5059.
- (5) Wang, X.; Horii, A.; Zhang, S. Designer Functionalized Self-Assembling Peptide Nanofiber Scaffolds for Growth, Migration, and Tubulogenesis of Human Umbilical Vein Endothelial Cells. *Soft Matter* **2008**, *4*, 2388–2395.
- (6) Kiyonaka, S.; Sugiyasu, K.; Shinkai, S.; Hamachi, I. First Thermally Responsive Supramolecular Polymer Based on Glycosylated Amino Acid. *J. Am. Chem. Soc.* **2002**, *124*, 10954–10955.
- (7) Adhikari, B.; Palui, G.; Banerjee, A. Self-Assembling Tripeptide Based Hydrogels and Their Use in Removal of Dyes from Waste-Water. *Soft Matter* **2009**, *5*, 3452–3460.
- (8) Chakraborty, P.; Roy, B.; Bairi, P.; Nandi, A. K. Improved Mechanical and Photophysical Properties of Chitosan Incorporated Folic Acid Gel Possessing the Characteristics of Dye and Metal Ion Absorption. *J. Mater. Chem.* **2012**, *22*, 20291–20298.
- (9) Vemula, P. K.; John, G. Smart Amphiphiles: Hydro/Organogelators for *In Situ* Reduction of Gold. *Chem. Commun.* **2006**, 2218–2220.

- (10) Kiyonaka, S.; Sada, K.; Yoshimura, S.; Shinkai, S.; Kato, N.; Hamachi, I. Semi-Wet Peptide/Protein Array Using Supramolecular Hydrogel. *Nat. Mater.* **2004**, *3*, 58–64.
- (11) Jhaveri, S. J.; McMullen, J. D.; Sijbesma, R.; Tan, L.-S.; Zipfel, W.; Ober, C. K. Direct Three-Dimensional Microfabrication of Hydrogels via Two-Photon Lithography in Aqueous Solution. *Chem. Mater.* **2009**, *21*, 2003–2006.
- (12) Babu, S. S.; Praveen, V. K.; Ajayaghosh, A. Functional  $\pi$ -Gelators and Their Applications. *Chem. Rev.* **2014**, *114*, 1973–2129.
- (13) Kartha, K. K.; Mukhopadhyay, R. D.; Ajayaghosh, A. Supramolecular Gels and Functional Materials Research in India. *Chimia* **2013**, *67*, 51–63.
- (14) Murdan, S. Electro-Responsive Drug Delivery from Hydrogels. *J. Controlled Release* **2003**, *92*, 1–17.
- (15) Abidian, M. R.; Martin, D. C. Multifunctional Nanobiomaterials for Neural Interfaces. *Adv. Funct. Mater.* **2009**, *19*, 573–585.
- (16) Lee, S. H.; Lee, C. K.; Shin, S. R.; Gu, B. K.; Kim, S. I.; Kang, T. M.; Kim, S. J. Enhanced Actuation of Ppy/CNT Hybrid Fibers Using Porous Structured DNA Hydrogel. *Sens. Actuators, B* **2010**, *145*, 89–92.
- (17) Fan, S.; Tang, Q.; Wu, J.; Hu, D.; Sun, H.; Lin, J. Two-Step Synthesis of Polyacrylamide/Poly(Vinyl Alcohol)/Polyacrylamide/Graphite Interpenetrating Network Hydrogel and Its Swelling, Conducting and Mechanical Properties. *J. Mater. Sci.* **2008**, *43*, 5898–5904.
- (18) Morita, S.; Kawai, T.; Yoshino, K. The Characteristics of a Conducting Polymer Gel by Use of a Radical Initiator. *J. Appl. Phys.* **1991**, *69*, 4445–4447.
- (19) Pépin-Donat, B.; Lairez, D.; de Geyer, A.; Viallat, A. Light and Small Angle Neutron Scattering Studies of Well-Defined Conducting Gels. *Synth. Met.* **1999**, *101*, 471–472.
- (20) Pépin-Donat, B.; Van-Quynh, A.; Viallat, A. Mechanisms of Deformation in Fully Conjugated Conducting Gels. Stretching and Swelling. *Macromolecules* **2000**, *33*, 5912–5917.
- (21) Pépin-Donat, B.; Viallat, A.; Blachot, J. F.; Fedorko, P.; Lombard, C. Swelling, Elasticity and Transport Properties of Conjugated Covalent Electronic Conducting Gels: Role of Network Structure. *Synth. Met.* **2003**, *137*, 897–898.
- (22) Jana, T.; Nandi, A. K. Sulfonic Acid-Doped Thermoreversible Polyaniline Gels: Morphological, Structural, and Thermodynamical Investigations. *Langmuir* **2000**, *16*, 3141–3147.
- (23) Jana, T.; Nandi, A. K. Sulfonic Acid Doped Thermoreversible Polyaniline Gels. 2. Influence of Sulfonic Acid Content on Morphological, Thermodynamical, and Conductivity Properties. *Langmuir* **2001**, *17*, 5768–5774.
- (24) Jana, T.; Chatterjee, J.; Nandi, A. K. Sulfonic Acid Doped Thermoreversible Polyaniline Gels. 3. Structural Investigations. *Langmuir* **2002**, *18*, 5720–5727.
- (25) Fizazi, A.; Moulton, J.; Pakbaz, K.; Rughooputh, S. D. D. V.; Smith, P.; Heeger, A. Percolation on a Self-Assembled Network: Decoration of Polyethylene Gels with Conducting Polymers. *J. Phys. Rev. Lett.* **1990**, *64*, 2180–2183.
- (26) González, I.; Vecino, M.; Muñoz, M. E.; Santamaría, A.; Pomposo, J. A. Electrically Conducting Gels Formed from Polyaniline/Ethylcellulose/m-Cresol Ternary Solutions. *Macromol. Chem. Phys.* **2004**, *205*, 1379–1384.
- (27) Zhang, Y. W.; Zhao, J. X.; Li, X. F.; Tao, Y.; Wu, C. X. Swelling Behaviors of Polyaniline-Poly(Acrylic Acid) Hydrogels. *J. Donghua Univ.* **2005**, *22*, 100–104.
- (28) Tang, Q. W.; Lin, J. M.; Wu, J. H.; Zhang, C. J.; Hao, S. C. Two-Steps Synthesis of a Poly(Acrylate-Aniline) Conducting Hydrogel with an Interpenetrated Networks Structure. *Carbohydr. Polym.* **2007**, *67*, 332–336.
- (29) Lin, J.; Tang, Q.; Hu, D.; Sun, X.; Li, Q.; Wu, J. Electric Field Sensitivity of Conducting Hydrogels with Interpenetrating Polymer Network Structure. *Colloids Surf., A* **2009**, *346*, 177–183.
- (30) Tang, Q.; Wu, J.; Sun, H.; Lin, J.; Fan, S.; Hu, D. Polyaniline/Polyacrylamide Conducting Composite Hydrogel with a Porous Structure. *Carbohydr. Polym.* **2008**, *74*, 215.
- (31) Xia, Y.; Zhu, H. Polyaniline Nanofiber-Reinforced Conducting Hydrogel with Unique pH Sensitivity. *Soft Matter* **2011**, *7*, 9388–9393.
- (32) Anilkumar, P.; Jayakannan, M. A Novel Supramolecular Organogel Nanotubular Template Approach for Conducting Nano-materials. *J. Phys. Chem. B* **2010**, *114*, 728–736.
- (33) Li, C.; Hatano, T.; Takeuchi, M.; Shinkai, S. Polyaniline Superstructures Created by a Templating Effect of Organogels. *Chem. Comm.* **2004**, 2350–2351.
- (34) Meng, L.; Lu, Y.; Wang, X.; Zhang, J.; Duan, Y.; Li, C. Facile Synthesis of Straight Polyaniline Nanostick in Hydrogel. *Macromolecules* **2007**, *40*, 2981–2983.
- (35) Chakraborty, P.; Bairi, P.; Roy, B.; Nandi, A. K. Improved Mechanical and Electronic Properties of Co-assembled Folic Acid Gel with Aniline and Polyaniline. *ACS Appl. Mater. Interfaces* **2014**, *6*, 3615–3622.
- (36) Ryan, D. M.; Nilsson, B. L. Self-Assembled Amino Acids and Dipeptides as Noncovalent Hydrogels for Tissue Engineering. *Polym. Chem.* **2012**, *3*, 18–33.
- (37) Sutton, S.; Campbell, N. L.; Cooper, A. I.; Kirkland, M.; Frith, W. J.; Adams, D. J. Controlled Release from Modified Amino Acid Hydrogels Governed by Molecular Size or Network Dynamics. *Langmuir* **2009**, *25*, 10285–10291.
- (38) Roy, S.; Banerjee, A. Amino Acid Based Smart Hydrogel: Formation, Characterization and Fluorescence Properties of Silver Nanoclusters within the Hydrogel Matrix. *Soft Matter* **2011**, *7*, 5300–5308.
- (39) Bairi, P.; Roy, B.; Routh, P.; Sen, K.; Nandi, A. K. Self-Sustaining, Fluorescent and Semi-Conducting Co-Assembled Organogel of Fmoc Protected Phenylalanine with Aromatic Amines. *Soft Matter* **2012**, *8*, 7436–7445.
- (40) Babu, S. S.; Prasanthkumar, S.; Ajayaghosh, A. Self-Assembled Gelators for Organic Electronics. *Angew. Chem., Int. Ed.* **2012**, *51*, 1766–1776.
- (41) Pana, L.; Yub, G.; Zhaia, D.; Leec, H. R.; Zhaod, W.; Liue, N.; Wang, H.; Teec, B.C.-K.; Shia, Y.; Cuid, Y.; Bao, Z. Hierarchical Nanostructured Conducting Polymer Hydrogel with High Electrochemical Activity. *Proc. Natl. Acad. Sci. U.S.A.* **2012**, *109*, 9287–9292.
- (42) Fatonia, A.; Numnuama, A.; Kanatharanaa, P.; Limbuta, W.; Thavarungkul, P. A Conductive Porous Structured Chitosan-Grafted Polyaniline Cryogel for use as a Sialic Acid Biosensor. *Electrochim. Acta* **2014**, *130*, 296–304.
- (43) Dawn, A.; Nandi, A. K. Formation of Silver Nanoparticles in Deoxyribonucleic Acid–Poly(o-methoxyaniline) Hybrid: A Novel Nano-biocomposite. *J. Phys. Chem. B* **2006**, *110*, 18291–18298.
- (44) Trchova, M.; Sedenkova, I.; Konyushenko, E. N.; Stejskal, J.; Holler, P.; Marjanovic, G. C. Evolution of Polyaniline Nanotubes: The Oxidation of Aniline in Water. *J. Phys. Chem. B* **2006**, *110*, 9461–9468.
- (45) Garai, A.; Kuila, B. K.; Nandi, A. K. Montmorillonite Clay Nanocomposites of Sulfonic Acid Doped Thermoreversible Polyaniline Gel: Physical and Mechanical Properties. *Macromolecules* **2006**, *39*, 5410–5418.
- (46) Palaniappan, S.; Nivasu, V. Emulsion Polymerization Pathway for Preparation of Organically Soluble Polyaniline Sulfate. *New. J. Chem.* **2002**, *26*, 1490–1494.
- (47) Stejskal, J.; Trchova, M.; Prokes, J.; Sapurina, I. Brominated Polyaniline. *Chem. Mater.* **2001**, *13*, 4083–4086.
- (48) Rana, U.; Chakrabarti, K.; Malik, S. In Situ Preparation of Fluorescent Polyaniline Nanotubes Doped with Perylene Tetracarboxylic Acids. *J. Mater. Chem.* **2011**, *21*, 11098–11100.
- (49) Stejskal, J.; Sapurina, I.; Trchová, M.; Konyushenko, E. N. Oxidation of Aniline: Polyaniline Granules, Nanotubes, and Oligoaniline Microspheres. *Macromolecules* **2008**, *41*, 3530–3536.
- (50) Rana, U.; Chakrabarti, K.; Malik, S. Benzene Tetracarboxylic Acid Doped Polyaniline Nanostructures: Morphological, Spectroscopic and Electrical Characterization. *J. Mater. Chem.* **2012**, *22*, 15665–15671.
- (51) Larson, R. G. *The Structure and Rheology of Complex Fluids*; Oxford University Press: New York, 1999.

- (52) Yan, C.; Pochanbe, D. J. Rheological Properties of Peptide-Based Hydrogels for Biomedical and Other Applications. *Chem. Soc. Rev.* **2010**, *39*, 3528–3540.
- (53) Chatterjee, S.; Layek, R. K.; Nandi, A. K. Changing the Morphology of Polyaniline from a Nanotube to a Flat Rectangular Nanopipe by Polymerizing in the Presence of Amino-Functionalized Reduced Graphene Oxide and Its Resulting Increase in Photocurrent. *Carbon* **2013**, *52*, 509–519.
- (54) Chang, S.-S.; Wu, C.-G. Effects of Polymerization Media on the Nanoscale Conductivity and Current–Voltage Characteristics of Chemically Synthesized Polyaniline Films. *J. Phys. Chem. B* **2005**, *109*, 18275–18282.
- (55) Genies, E. M.; Lapkowski, M. Influence of Light on the Electrochemical Behaviour of Polyaniline Films. *Synth. Met.* **1988**, *24*, 69–76.
- (56) Karmakar, A.; Ghosh, A. Charge Carrier Dynamics and Relaxation in (Polyethylene Oxide–Lithium-Salt)-Based Polymer Electrolyte Containing 1-Butyl-1-methylpyrrolidinium Bis(trifluoromethylsulfonyl)imide as Ionic Liquid. *Phys. Rev. E* **2011**, *84*, 051802.
- (57) Dias, F. B.; Plomp, L.; Veldhuis, J. B. J. Trends in Polymer Electrolytes for Secondary Lithium Batteries. *J. Power Sources* **2000**, *88*, 169–191.
- (58) Rubinson, J. F.; Kayinamura, Y. P. Charge Transport in Conducting Polymers: Insights from Impedance Spectroscopy. *Chem. Soc. Rev.* **2009**, *38*, 3339–3347.
- (59) Kalpana, D.; Renganathan, N. G.; Pitchumani, S. A New Class of Alkaline Polymer Gel Electrolyte for Carbon Aerogel Supercapacitors. *J. Power Sources* **2006**, *157*, 621–623.
- (60) Campbell, A. J.; Bradley, D. D. C.; Lidzey, D. G. Space-Charge Limited Conduction with Traps in Poly(Phenylene Vinylene) Light Emitting Diodes. *J. Appl. Phys.* **1997**, *82*, 6326–6342.
- (61) Hui, D.; Alexandrescu, R.; Chipara, M.; Morjan, I.; Aldica, G.; Chipara, M. D.; Lau, K. T. Impedance Spectroscopy Studies on Doped Polyanilines. *J. Optoelectron. Adv. Mater.* **2004**, *6*, 817–824.
- (62) Onwudiwe, D. C.; Arfin, T.; Strydom, C. A.; Kriek, R. J. A Study of the Thermal and AC Impedance Properties of N-Phenyl-dithiocarbamate Complexes of Zn(II). *Electrochim. Acta* **2013**, *109*, 809–817.
- (63) Bekin, S.; Sarmad, S.; Gurkan, K.; Yenici, G.; Keceli, G.; Gurdag, G. Dielectric, Thermal, and Swelling Properties of Calcium Ion-Crosslinked Sodium Alginate Film. *Polym. Eng. Sci.* **2014**, *54*, 1372–1382.